Nano Research

Open Access

Research Article

PIN quantum-dot LEDs with enhanced efficiency and stability enabled by bulk-heterojunction hole transport layer

Heng Zhang[1,§] ✉, Zhe Wang[1,§], Dawei Yang[1], Bingsuo Zou[1] ✉, and Shuming Chen[2] ✉

[1] School of Resources, Environments and Materials, Guangxi University, Nanning 530004, China
[2] Department of Electrical and Electronic Engineering, Southern University of Science and Technology, Shenzhen 518055, China
[§] Heng Zhang and Zhe Wang contributed equally to this work.

Cite this article: *Nano Research*, **2025**, *18*, 94907155. https://doi.org/10.26599/NR.2025.94907155

ABSTRACT: Although quantum-dot light-emitting diodes (QLEDs) can exhibit high efficiency and long lifetime, the realization of QLEDs-based displays remains challenging due to their complex multilayer architectures and the use of unstable poly(3,4-ethylenedioxythiophene):poly(styrene sulfonate) (PEDOT:PSS) hole injection layer (HIL). Here, we develop a novel trilayer p-type/intrinsic/n-type (PIN) QLED with only three functional layers: PTAA:TFB:F4-TCNQ (PTAA: poly[bis(4-phenyl)(2,4,6-trimethylphenyl)amine]; TFB: poly[(9,9-dioctylfluorenyl-2,7-diyl)-co-(4,4'-(N-(4-sec-butylphenyl)diphenylamine)]; F4-TCNQ: 2,3,5,6-tetrafluoro-7,7,8,8-tetracyanoquinodimethane) bulk-heterojunction (BHJ) hole transport layer (HTL), quantum-dot emitting layer, and ZnMgO electron transport layer. Due to well-matched energy level, increased hole transport path from PTAA to TFB, and improved hole density and enhanced hole mobility of the PTAA:TFB:F4-TCNQ BHJ HTL, the resultant trilayer PIN QLED exhibits a high external quantum efficiency (EQE) of 25.1% and an impressive peak brightness of 382,600 cd/m^2, which are significantly higher than those of the control QLED. Moreover, the trilayer PIN QLED also shows a 1.94-fold longer operational lifetime than control QLED due to the improved device performance, reduced charge accumulation, and removal of unstable PEDOT:PSS. The developed trilayer PIN QLED, with fewer functional layers and better stability, could promote the practical application of QLED in displays and solid-state lighting.

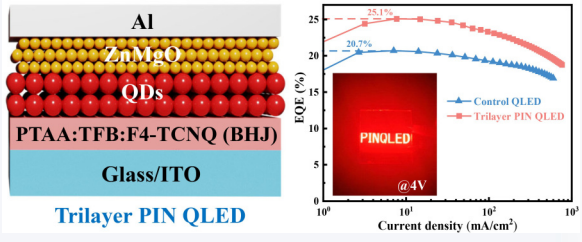

KEYWORDS: quantum dots, light-emitting diodes, trilayer, hole transport layer, p-type/intrinsic/n-type (PIN)

1 Introduction

Quantum dot light-emitting diodes (QLEDs) have become excellent light sources for flat-panel displays and solid-state lighting due to their fascinating merits of high color saturation, tunable emission wavelength, and facile solution processability [1–8]. Recent advancements have demonstrated that the external quantum efficiencies (EQEs) of red (R-), green (G-), and blue (B-) QLEDs have surpassed 20%, and the T_{95} operational lifetimes (the time when the brightness drops to 95% of the initial value) of R- and G-QLEDs have reached 48,000 and 7200 h at an initial brightness (L_0) of 1000 cd/m^2, respectively [9–14]. Although these performances have fulfilled the requirements of display applications, the practical application of QLEDs in displays remains challenging.

One challenge is that QLED shows a complex multilayer architecture, which is not conducive to mass production. Similar to the organic light-emitting diode (OLED), typical QLED consists of a sequentially stacked multiple functional layers, including a hole injection layer (HIL), hole transport layer (HTL), quantum-dot emitting-layer (QD-EML), and electron transport layer (ETL) [15–19]. Additionally, an electron blocking layer (EBL) is further employed in some high-performance QLEDs to improve charge injection balance [20–22]. Although device performance can be improved by increasing the number of functional layers, it also introduces significant shortcomings. Firstly, the presence of multiple functional layers leads to the formation of multiple interfaces; as the injected charges could accumulate at each interface, the increase in the number of interfaces results in severe charge accumulation that eventually degrades the performance of QLEDs. Secondly, because it is far from mature to fabricate large-sized and uniform functional layers (< 50 nm) by solution-processing, additional functional layers will inevitably decrease the manufacturing yield of the devices. Thirdly, the increase in the

Received: September 25, 2024; **Revised:** November 3, 2024
Accepted: November 25, 2024

✉Address correspondence to Heng Zhang, zhangheng@gxu.edu.cn; Bingsuo Zou, zoubs@gxu.edu.cn; Shuming Chen, chen.sm@sustech.edu.cn

number of functional layers also complicates the device fabricating process, resulting in increased manufacturing costs and manufacturing time.

Another challenge is that the conductive polymer poly(3,4-ethylenedioxythiophene):poly(styrene sulfonate) (PEDOT:PSS), which is commonly employed as HIL of QLED, exhibits high hygroscopicity and acidity [23–28], limiting the long-term operational stability of QLEDs. It should be noted that because most reported lifetime data were extrapolated from short-term (< ~ 30 days) measurements conducted under high brightness [14, 29–32], the acidic and hygroscopic nature of PEDOT:PSS was not considered in the reported long-lifetime QLEDs. Highly stable inorganic metal oxides such as V_2O_5, WO_3, MoO_3, and NiO_x are usually employed instead of PEDOT:PSS as HIL to improve device stability [33–39], but the device performance is limited due to their inferior hole injection capability caused by low conductivity and/or interface defects.

To address the aforementioned challenges, we herein demonstrate a novel trilayer p-type/intrinsic/n-type (PIN) QLED consisting of only three functional layers, which are p-type PTAA:TFB:F4-TCNQ (PTAA: poly[bis(4-phenyl)(2,4,6-trimethylphenyl)amine]; TFB: poly[(9,9-dioctylfluorenyl-2,7-diyl)-co-(4,4'-(N-(4-sec-butylphenyl)diphenylamine)]; F4-TCNQ: 2,3,5,6-tetrafluoro-7,7,8,8-tetracyanoquinodimethane) bulk-heterojunction (BHJ) HTL, QD-EML, and n-type ZnMgO ETL. The PTAA:TFB:F4-TCNQ BHJ HTL, which is a ternary hybrid HTL consisting of PTAA, TFB, and F4-TCNQ, can replace the role of traditional PEDOT:PSS/TFB HIL/HTL due to its excellent hole injection capability caused by well-matched energy level, increased hole transport path from PTAA to TFB, and improved hole density and hole mobility. With the PTAA:TFB:F4-TCNQ BHJ HTL, the number of functional layers can be reduced. Meanwhile, the resultant trilayer PIN QLED can exhibit an excellent EQE of 25.1% and an impressive peak luminance of 382,600 cd/m^2, which are significantly higher than those of control QLED. Moreover, the trilayer PIN QLED also shows 1.94-fold longer operational lifetimes and 3.01-fold longer shelf-lifetimes than control QLED due to the improved device performance, reduced charge accumulation, and removal of unstable PEDOT:PSS. We believe that the demonstrated efficient and bright trilayer PIN QLED, with fewer functional layers and better stability, could advance the commercialization of QLED technology.

2 Results and discussion

2.1 Structure and working mechanism of PIN QLED

As shown in Fig. 1(a), the structure of trilayer PIN QLED is ITO/PTAA:TFB:F4-TCNQ/QDs/ZnMgO/Al (ITO: indium tin oxide), where the PTAA:TFB:F4-TCNQ BHJ HTL is a hybrid film

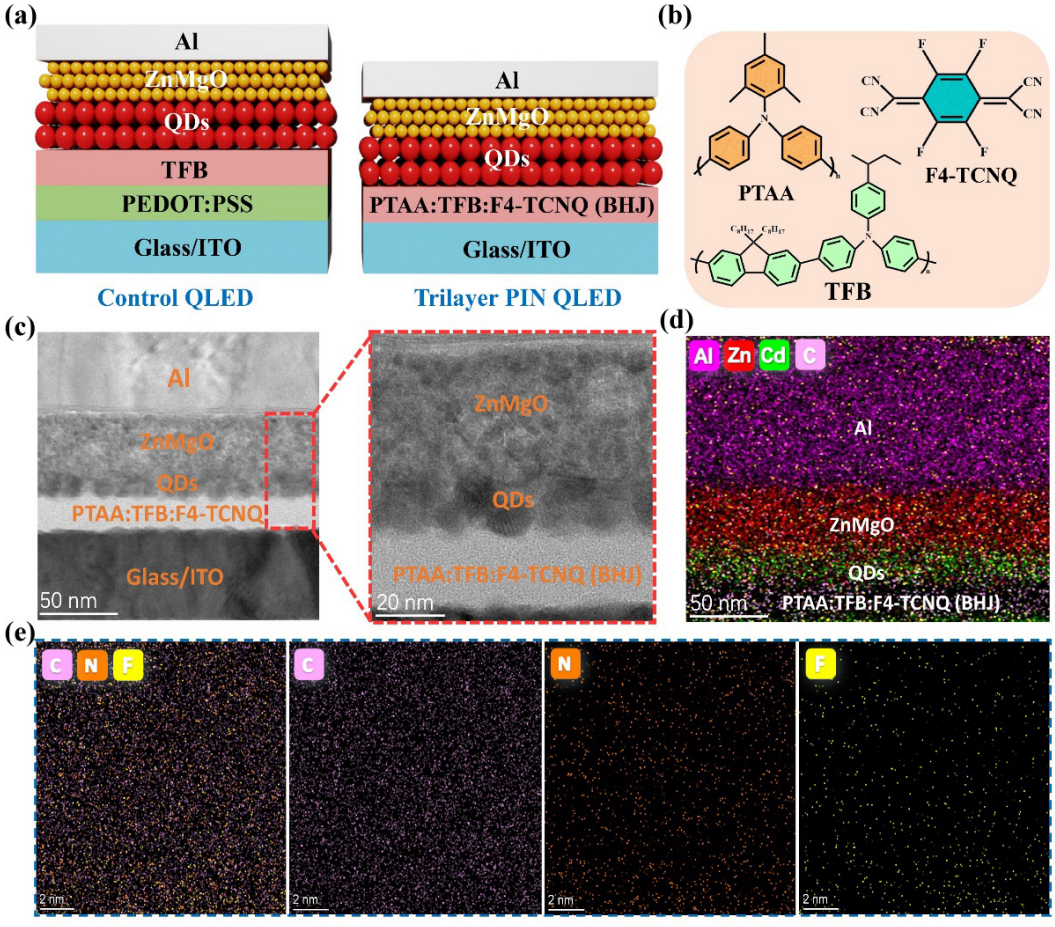

Figure 1 Device structure of trilayer PIN QLED. (a) Schematic device structures of the control QLED and trilayer PIN QLED. (b) Schematic chemical structures of PTAA, TFB, and F4-TCNQ. (c) Cross-sectional TEM images of the trilayer PIN QLED with scale bars of 50 and 20 nm. (d) Cross-sectional color-mixed elemental mapping image of Al, Zn, Cd, and C detected by EDS. (e) Zoomed-in (with the scale bar of 2 nm) cross-sectional elemental mapping images of C, N, and F of the PTAA:TFB:F4-TCNQ BHJ HTL detected by EDS.

composed of PTAA (polymer), TFB (polymer), and F4-TCNQ (small molecule). In the PTAA:TFB:F4-TCNQ BHJ HTL, PTAA is employed to reduce the hole injection barrier between ITO and TFB, TFB is utilized to transport the injected hole to QDs, and F4-TCNQ serves as p-type electron acceptor dopant to enhance hole mobility of the HTL, which will be discussed later. Except the PTAA:TFB:F4-TCNQ BHJ HTL, all other layers of trilayer PIN QLED are identical to those of control QLED. The detailed molecular structures of PTAA, TFB, and F4-TCNQ are shown in Fig. 1(b). To confirm the device architecture, the morphology of the cross-section of a device was first studied by the transmission electron microscopy (TEM). As shown in Fig. 1(c), only three layers between ITO and Al electrodes can be observed, confirming that the device consists of only three functional layers. The elemental composition of these functional layers was further examined by the energy-dispersive X-ray spectroscopy (EDS). As shown in Fig. 1(d) and Fig. S1 in the Electronic Supplementary Material (ESM), both area-scan and line-scan results indicate that the observed three functional layers are PTAA:TFB:F4-TCNQ, QDs, and ZnMgO, respectively.

To further explore the morphology of PTAA:TFB:F4-TCNQ BHJ HTL, the distribution of PTAA, TFB, and F4-TCNQ in the film was also studied. As shown in Fig. S2 in the ESM, the PTAA, TFB, and F4-TCNQ can be distributed uniformly (without phase separation) in solutions, and thus the homogeneously mixed PTAA:TFB:F4-TCNQ BHJ film was fabricated by the solution processing. Figure 1(e) shows the zoomed-in (with a scale bar of 2 nm) cross-sectional elemental mapping images of PTAA:TFB:F4-TCNQ BHJ HTL. The uniform random distribution of C, N, and F elements reveals that PTAA, TFB, and F4-TCNQ are uniformly distributed in the film, further confirming that PTAA, TFB, and F4-TCNQ are homogeneously mixed in PTAA:TFB:F4-TCNQ BHJ HTL.

Figure 2(a) shows the charge injection process in trilayer PIN QLED. Same as control QLED, electrons can be directly injected through the conduction band (CB) of ZnMgO and subsequently transported to CB of QDs. The hole injection process can be divided into three parts. Firstly, under an electric field, the holes in anode can be preferential injected into the highest occupied molecular orbital (HOMO) level of PTAA (~ 5.1 eV) due to the lower hole injection barrier between ITO (~ 4.7 eV) and PTAA. Secondly, because of well-matched HOMO levels of PTAA and TFB (~ 5.3 eV), the injected holes can be smoothly transferred to HOMO level of TFB in PTAA:TFB:F4-TCNQ BHJ HTL. Finally, similar to control QLED, the holes in TFB can be further transferred to the valence band (VB) of QDs to combine with the injected electrons. As shown in Fig. 2(b), the intermolecular charge transfer process, which is electrons on HOMO level of PTAA or TFB transferred to the lowest unoccupied molecular orbital (LUMO) level of F4-TCNQ, also occurs in PTAA:TFB:F4-TCNQ BHJ HTL during the charge injection process, thereby making the holes more efficiently injected into QDs. From this working mechanism, the basic principles of the BHJ HTL design can be summarized. Firstly, to obtain uniform BHJ HTL through solution processing, the most ideal approach is to select multiple organic materials that can be dissolved simultaneously in the same solvent. Secondly, because TFB has been proven to be effective in transferring holes into QDs, it is necessary to obtain hole injection materials that match the work functions of ITO and HOMO level of TFB to ensure that holes can be effectively injected from ITO to TFB. Finally, due to excessive electron injection in QLED, it is also necessary to further enhance the hole injection capability of HTL by doping p-type electron acceptor materials, which exhibit a LUMO level close to the HOMO level of both TFB and hole injection materials.

2.2 High-performance PIN QLED

As shown in Fig. 3(a), the trilayer PIN QLED exhibits a bright and pure red emission, and its electroluminescent (EL) spectra, with a peak position at 632.68 nm and a narrow full width at half maximum of 23.72 nm, are identical to those of the control QLED. The current density (J)–voltage (V)–luminance (L) characteristics of the most efficient trilayer PIN QLED and control QLED are compared in Fig. 3(b). It can be observed that at the same driving voltage, the current density of trilayer PIN QLED is significantly higher than that of control QLED, indicating that hole injection of PTAA:TFB:F4-TCNQ BHJ HTL is more efficient than PEDOT:PSS/TFB HIL/HTL. As a result, the trilayer PIN QLED exhibits an excellent EQE of 25.07% and an impressive peak brightness of 382,600 cd/m^2, which are significantly higher than those of control QLED (Figs. 3(b) and 3(c), and Fig. S3(a) in the ESM). As shown by the histograms for 12 devices from different batches (Fig. 3(d)), the average peak EQE of trilayer PIN QLED, 23.99%, is about 1.19-fold higher than 20.08% of the control QLEDs, demonstrating that the higher performance of trilayer PIN QLED is highly repeatable. As shown in Fig. 3(e), the trilayer PIN QLED exhibits an ultralong T_{95} operational lifetime of 84.67 h at 16,500 cd/m^2 (corresponding to 5675 h or 236.5 days at

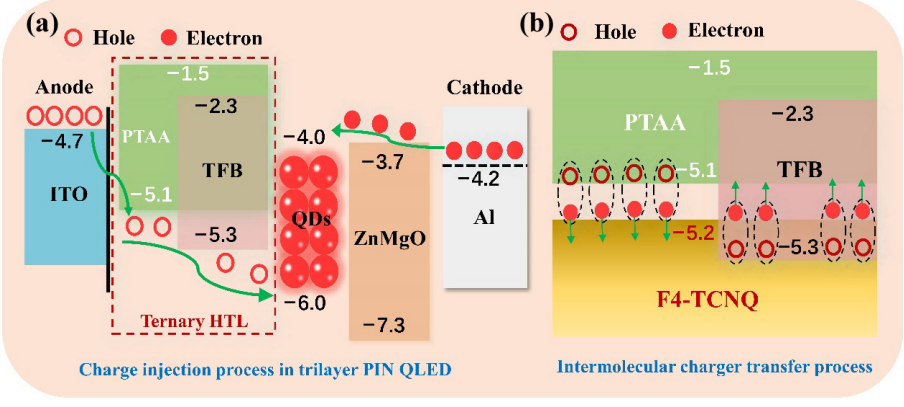

Figure 2 Working mechanism of trilayer PIN QLED. (a) Schematic diagram of the charge injection process in trilayer PIN QLED. (b) Schematic diagram of the intermolecular charge transfer process in PTAA:TFB:F4-TCNQ BHJ HTL.

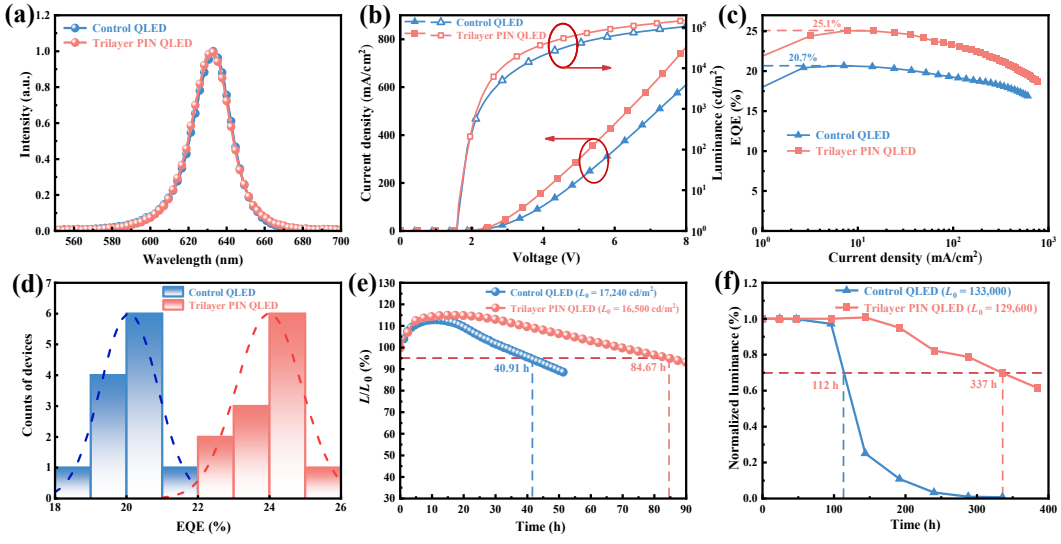

Figure 3 Comparison of the performances of trilayer PIN QLED and control QLED. (a) Normalized EL spectra of the devices. The inset demonstrates a photograph of a patterned trilayer PIN QLED driven at 4 V. (b) *J*–*V*–*L* and (c) EQE–*L* characteristics of the devices. (d) Histograms of the maximum EQEs of the devices (each obtained from 12 devices). (e) Operational lifetimes of the devices (40.91 h at 17,240 cd/m² for control QLED and 84.67 h at 16,500 cd/m² for trilayer PIN QLED). (f) Normalized *L*-time (*T*) characteristics of the devices (turn–off) stored under ambient conditions over an extended period.

1000 cd/m²), which is remarkably longer than that of control QLEDs (40.91 h at 17,240 cd/m²). Moreover, as shown in Fig. 3(f), the T_{70} (the time when the brightness drops to 70% of the initial value) shelf-lifetime of the trilayer PIN QLED (337 h at 129,600 cd/m²) is about 3-fold longer than that of control QLEDs (112 h at 133,000 cd/m²). We believe that these remarkably improved operational lifetime and shelf-lifetime of the trilayer PIN QLEDs are mainly due to the enhanced device performance, mitigated charge accumulation, and removal of unstable PEDOT:PSS. The detailed performances of trilayer PIN QLEDs and control QLEDs are compared in Figs. S3(b), S3(c), and S4 in the ESM, as well as Table 1.

As shown in Fig. S5 in the ESM, when the ratio of PTAA:TFB increases from 0:1 to 0.4:1, the device performance gradually increases, which is mainly due to the enhancement of hole injection from ITO to TFB through PTAA; while when the ratio of PTAA:TFB continually increases (> 0.4:1), the device performance gradually decreases, which is mainly due to the suppression of hole transport from TFB to QDs caused by the reduction of TFB content. In addition to the PTAA:TFB ratio, the device performance is also significantly affected by the F4-TCNQ content. As shown in Fig. S6 in the ESM, when the F4-TCNQ content increases from 0% to 0.25%, the device performance is remarkably improved, which is mainly due to the further enhanced hole injection of PTAA:TFB by introducing F4-TCNQ. However, excessive F4-TCNQ content (> 0.25%) will lead to a decrease of PTAA:TFB content, which is not conducive to hole injection, thereby leading to the decrease of device performance. The optimal PTAA:TFB:F4-TCNQ weight ratio and thickness of the PTAA:TFB:F4-TCNQ BHJ HTL, which can be concluded from the device performances in Figs. S5–S7 in the ESM, are 28.50:71.25:0.25 and 35 nm, respectively. It should be noted that although the device structure can be simplified by using PTAA:TFB:F4-TCNQ BHJ HTL, its performance is sensitive to the ratio of each component in the HTL, which indicates that precise control of the ratio of PTAA:TFB:F4-TCNQ is crucial and challenging.

2.3 Mechanism of high-performance of the trilayer PIN QLED

To investigate the mechanism for performance improvement of trilayer PIN QLED, the performances of QLEDs with different HTLs or HIL/HTL are compared in Fig. S8 in the ESM, and the energy levels of the HTLs are also examined (Fig. S9 and Table S1 in the ESM). It can be seen that the performances of PTAA:TFB HTL based device are remarkably higher than pure TFB HTL based device, and by incorporating F4-TCNQ, the device performances can be further improved, which are higher than conventional PEDOT:PSS/TFB HIL/HTL based device. The stepwise performance improvement of these trilayer PIN QLEDs is mainly due to the improved charge injection balance, which can be verified by the reduced capacitance of the devices (Fig. 4(a)).

Because electrons are over-injected in red QLEDs, the improved charge injection balance is mainly attributed to the mitigation of electron leakage and/or the enhancement of hole injection. As shown in Fig. 4(b), the TFB emission in EL spectra of trilayer PIN QLED is remarkably weaker than that of control QLED at the same current density, indicating that the electron leakage is significantly suppressed in trilayer PIN QLED, which can be further confirmed

Table 1 Detailed performances of trilayer PIN QLED and control QLED

Device	Max. brightness (cd/m²)	Max. EQE (%)	Max. current efficiency (cd/A)	Max. power efficiency (lm/W)	T_{95} operational lifetime		T_{70} shelf lifetime
Control QLED	339,700	20.7	21.2	32.1	40.91 h @17,240 cd/m²	2928 h @1000 cd/m²	112 h @133,000 cd/m²
Trilayer PIN QLED	382,600	25.1	25.6	37.2	84.68 h @16,500 cd/m²	5675 h @1000 cd/m²	337 h @129,600 cd/m²

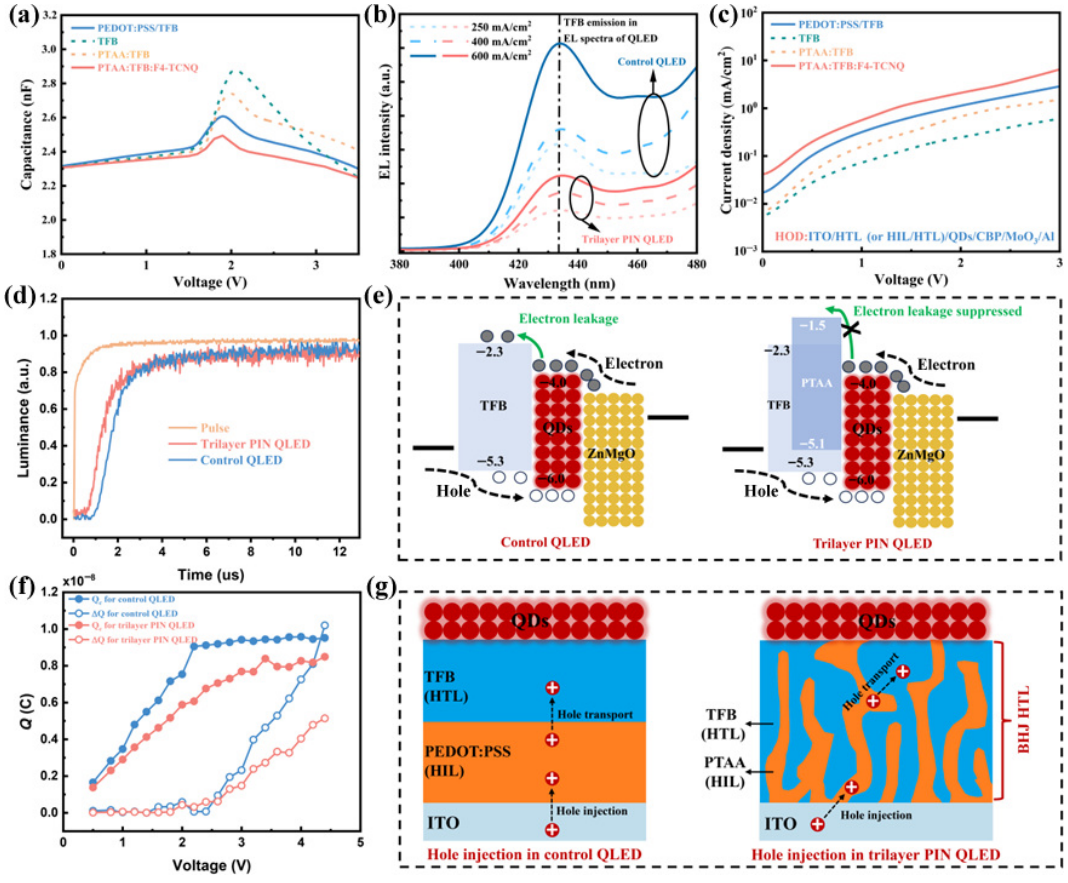

Figure 4 Mechanism of high-performance of the trilayer PIN QLED. (a) *C*–*V* characteristics of the QLEDs with different HTL or HIL/HTL. (b) TFB emissions in EL spectra of control QLED and trilayer PIN QLED driven at different current densities (250, 400, and 600 mA/cm²). (c) *J*–*V* characteristics of HODs with structure of ITO/HTL (or HIL/HTL)/QDs/CBP/MoO_3/Al. (d) TrEL spectra of control QLED and trilayer PIN QLED. (e) Schematic diagram of the mechanism for suppressing electron leakage in trilayer PIN QLED. (f) Calculated Q_c–*V* and Δ*Q*–*V* curves of control QLED and trilayer PIN QLED. (g) Schematic diagram of the mechanism for enhancing hole transport from HIL to HTL in trilayer PIN QLED.

by the lower current density of the trilayer PIN QLED (with PTAA:TFB:F4-TCNQ BHJ HTL) driven at low voltages (Fig. S10 in the ESM). To verify the enhancement of hole injection, hole-only devices (HODs) were prepared and investigated. As shown in Fig. 4(c), the current density of PTAA:TFB-based device is larger than that of TFB-based device, and by using PTAA:TFB:F4-TCNQ as HTL, the device current density can be further improved, indicating that the hole injection is enhanced by incorporating PTAA and F4-TCNQ into TFB HTL. Because the hole is a minority carrier in QLED, hole injection capability can also be evaluated by detecting the rising time of the transient electroluminescence (TrEL) [40–43]. As shown in Fig. 4(d), the EL rise time of trilayer PIN QLED, ~ 4.5 μs, is significantly lower than that of control QLED (~ 5.1 μs), further confirming that the hole injection is enhanced in trilayer PIN QLED.

As shown in Fig. 4(e), because the LUMO level of PTAA is −1.5 eV, which is lower than that of TFB (−2.3 eV), the electrons injected into QDs can be more efficiently blocked in trilayer PIN QLED. Consequently, the main reason for the suppression of electron leakage is the adoption of PTAA. In terms of the enhancement of hole injection, there are mainly three reasons.

(I) The hole transport from HIL to HTL is improved. Because the injected holes are easily accumulated at the interface of HIL/HTL (PTAA/TFB or PEDOT:PSS/TFB) in QLED [44], the enhanced hole transport from HIL to HTL can be verified by the reduced hole accumulation. To investigate the hole accumulation, the time-resolved current (TRC) measurements were performed. As shown in Fig. 4(f), the calculated Q_c value (charges accumulated on the QLED capacitor) of trilayer PIN QLED is significantly lower than that of control device, indicating that the charges (electrons and holes) accumulated on trilayer PIN QLED capacitor are significantly less than those accumulated on control QLED capacitor [44]. Because the QDs/ETL interface of trilayer PIN QLED is identical to that of control QLED, the decreased charge accumulation is mainly attributed to the reduction of hole accumulation, which confirms the enhancement of hole transport from HIL to HTL. It can also be seen that the trilayer PIN QLED shows a lower Δ*Q* value (charges accumulated on emitting layer) than control QLED, indicating that the charge injection in trilayer PIN QLED is more balanced than that in control QLED, which is mainly due to the enhanced hole injection. Because the HOMO level of PTAA is similar to that of PEDOT:PSS (~ 5.1 eV), which aligns well with the work function of ITO, holes can be efficiently injected from ITO into PTAA or PEDOT:PSS. As shown in Fig. 4(g), since PTAA and TFB are evenly mixed in trilayer PIN QLED, the interface area between them is significantly larger than that between PEDOT:PSS and TFB in control device. Consequently, the hole transport paths from HIL to HTL are remarkably increased in trilayer PIN QLED, thus significantly enhancing the hole injection from ITO to QDs.

(II) The hole density of HTL is increased. The F4-TCNQ, with the LUMO of ~ 5.2 eV, was commonly employed as p-type electron acceptor dopant to improve hole density of the HTL, and thus we believe that the hole density of binary PTAA:TFB BHJ HTL can be improved by introducing F4-TCNQ. As shown in Fig. S11 in the ESM, because the LUMO level of F4-TCNQ is very close to the HOMO level of PTAA or TFB, the electrons in HOMO level of PTAA or TFB can be smoothly transferred to LUMO level of F-TCNQ through the integer charge transfer (ICT) process, thereby increasing the hole density of PTAA or TFB. To investigate whether hole concentration is varied, the work functions of PTAA, PTAA:F4-TCNQ, TFB, and TFB:F4-TCNQ films were studied by Kelvin probe (KP). As shown in Fig. 5(a), the work functions of both PTAA and TFB downshift (from −3.26 to −3.44 and from −3.67 to −3.74 eV, respectively) by introducing F4-TCNQ. Benefiting from the downshifted Fermi energy level, hole density below the HOMO level of both PTAA:F4-TCNQ and TFB:F4-TCNQ would multiply (the schematic diagram shown in Fig. 5(b)), thus enabling PTAA:F4-TCNQ and TFB:F4-TCNQ to show higher hole concentration than pure PTAA and TFB, respectively.

(III) The hole mobility of HTL is enhanced. Because the F4-TCNQ can serve as the electron hopping sites, we believe that the hole mobility of the binary PTAA:TFB BHJ HTL can also be enhanced by doping F4-TCNQ. Indeed, as shown in Fig. 5(c), the hole mobilities of PTAA:F4-TCNQ and TFB:F4-TCNQ, which are extracted from *J*–*V* curves of the HODs (Fig. S12 in the ESM) by using space-charge-limited current (SCLC) theory, are significantly higher than pure PTAA and TFB, respectively. Because the hole mobilities of PTAA and TFB can be enhanced by incorporating F4-TCNQ, the ternary PTAA:TFB:F4-TCNQ BHJ HTL exhibits a remarkably higher hole mobility (8.01×10^{-5} cm^2/(V·s)) than that of binary PTAA:TFB BHJ HTL (3.68×10^{-5} cm^2/(V·s)). Since the hole mobility can also be determined by the molecular orientation and crystalline behaviors of PTAA:TFB:F4-TCNQ BHJ HTL, grazing incidence wide-angle X-ray scattering (GIWAXS) characterizations were also conducted, as shown in Figs. 5(d)–5(f). The observed annular GIWAX patterns and (010) peaks (at 1.68 and 1.88 Å^{-1} for PTAA:TFB:F4-TCNQ and TFB, respectively) in the in-plane (IP) and out-of-plane (OOP) directions indicate that both TFB and PTAA:TFB:F4-TCNQ films show mixed edge-on and face-on orientation. The calculated (010) coherence length of PTAA:TFB:F4-TCNQ, which is determined by the diffraction peak, is 8.05 Å, which is higher than 7.35 Å of TFB, suggesting that molecular stacking in PTAA:TFB:F4-TCNQ is more ordered. Moreover, a new diffraction peak at 0.22 Å^{-1}, which is mainly caused by PTAA (see Fig. S13 in the ESM), can be observed in OOP direction of PTAA:TFB:F4-TCNQ, indicating that a more ordered lamellar stacking formed in PTAA:TFB:F4-TCNQ film. These results demonstrate that PTAA:TFB:F4-TCNQ BHJ HTL shows a better molecular stacking order than traditional TFB HTL, which also contributes to the increased hole mobility observed in PTAA:TFB:F4-TCNQ BHJ HTL.

Because the surface morphology of HTL significantly affects device performances, the height images of different organic films were further detected by atomic force microscopy (AFM), as shown in Fig. S14 in the ESM. All films, including PTAA, TFB, F4-TCNQ, PTAA:TFB, and PTAA:TFB:F4-TCNQ, exhibit a low surface roughness with root mean square (Rq) of < 5 nm, indicating that the surface morphology of PTAA:TFB:F4-TCNQ BHJ HTL is not deteriorated by the integration of multiple organic materials. On the contrary, the surface morphology of PTAA:TFB:F4-TCNQ BHJ HTL (Rq = 0.434) is even better than conventional TFB HTL (Rq = 0.451), which may be due to the more ordered molecular stacking in PTAA:TFB:F4-TCNQ. Because of similar surface morphology, the exciton quenching efficiency at the interface of PTAA:TFB:F4-TCNQ/QDs or TFB/QDs is almost the same (Fig. S15 in the ESM). As shown in Figs. S16 and S17 in the ESM, although PTAA:TFB:F4-TCNQ BHJ HTL can exhibit higher transmittance than conventional PEDOT:PSS/TFB HIL/HTL, the light out-coupling efficiency of trilayer PIN QLED (24.4%) is even lower than that of

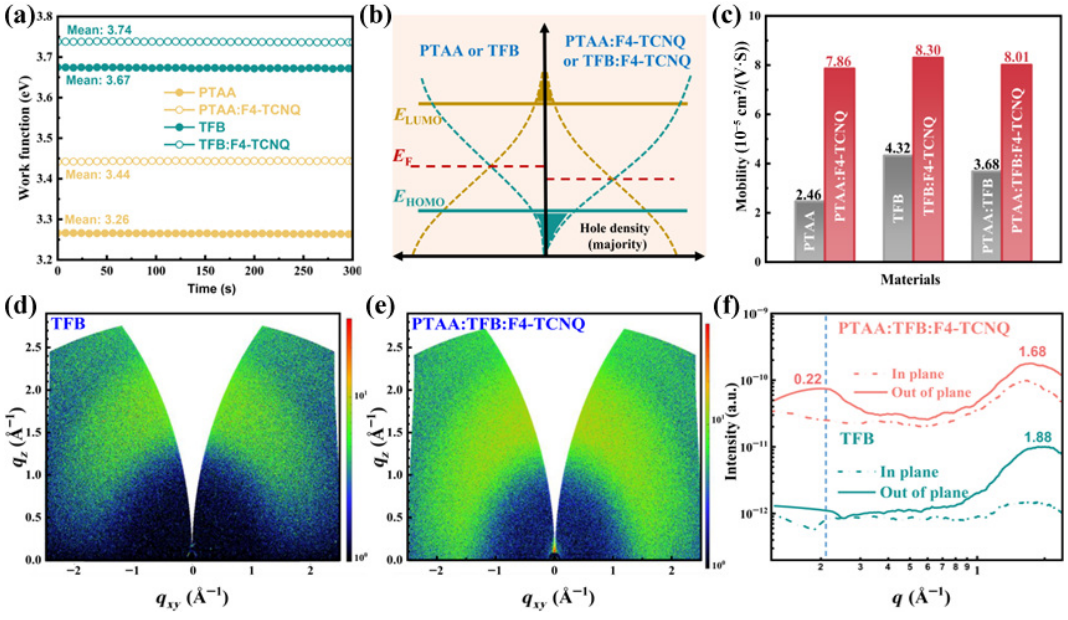

Figure 5 Mechanism of hole density and hole mobility enhancement in PTAA:TFB:F4-TCNQ BHJ HTL. (a) Work function of different films calculated by using the contact potential difference (CPD) results measured by Kelvin probe. The ITO (considering the work function at 4.7 eV) is employed as a reference specimen. (b) Schematic electronic structure of PTAA:F4-TCNQ or TFB:F4-TCNQ. (c) Charge mobilities of different films. Two-dimensional (2D) GIWAXS patterns of TFB (d) and PTAA:TFB:F4-TCNQ BHJ HTL (e). (f) IP and OOP profiles extracted from 2D GIWAXS patterns in (b) and (c).

control QLED (28.4%), indicating that the high-performance of trilayer PIN QLED mainly comes from the improved electrical performance of the PTAA:TFB:F4-TCNQ BHJ HTL.

From the aforementioned studies, we can conclude that the improvement of the luminance efficiency of trilayer PIN QLED is mainly attributed to the effective suppression of electron leakage and enhancement of hole injection. Although the improved efficiency can contribute to the device stability, we believe that the remarkably improved device stability is also attributed to two other reasons. One reason is the removal of unstable PEDOT:PSS, which contributes to the stability of the ITO anode and functional layers. Another reason is the reduction of hole accumulation at the interface of HIL/HTL, which can alleviate the damage of the accumulated charges to the electrical performance of the TFB HTL. This result can be verified by the lower driving voltage of the trilayer PIN QLED during the lifetime measurements, as shown in Fig. S18 in the ESM.

3 Conclusions

In summary, an efficient and bright trilayer PIN QLED with a structure of ITO/PTAA:TFB:F4-TCNQ/QDs/ZnMgO/Al is developed, where PTAA:TFB:F4-TCNQ is a BHJ HTL consisting of PTAA, TFB, and F4-TCNQ. Due to the effective improvement of hole transport path from PTAA to TFB, reduction of hole injection barrier by PTAA, and enhancement of hole concentration and hole mobility by F4-TCNQ, the PTAA:TFB:F4-TCNQ BHJ HTL exhibits better hole injection capability than conventional PEDOT:PSS/TFB HIL/HTL. In addition, compared with PEDOT:PSS/TFB HIL/HTL, the PTAA:TFB:F4-TCNQ BHJ HTL also shows better surface morphology and higher transmittance. As a result, the obtained trilayer PIN QLED exhibits an excellent EQE of 25.1% and an impressive maximum brightness of 382,600 cd/m^2, which are remarkably higher than those of control QLED. Furthermore, due to the improved device performance, reduced charge accumulation, and removal of unstable PEDOT:PSS, the trilayer PIN QLED also show a T_{95} operational lifetime of 5675 h (L_0 = 1000 cd/m^2) and a T_{70} shelf-lifetime of 337 h (L_0 = 129,600 cd/m^2), which are significantly higher than 2928 (L_0 = 1000 cd/m^2) and 112 h (L_0 = 133,000 cd/m^2) of control QLED, respectively. We believe that the demonstrated high-performance trilayer PIN QLED, with fewer functional layers and better stability, could promote the practical application of QLED technology in displays and solid-state lighting.

4 Method

4.1 Device structures

(1) Trilayer PIN QLED: ITO (110 nm)/PTAA:TFB:F4-TCNQ (35 nm)/QDs (20 nm)/ZnMgO (50 nm)/Al (100 nm).

(2) Control QLED: ITO (110 nm)/PEDOT:PSS (40 nm)/TFB (40 nm)/QDs (20 nm)/ZnMgO (50 nm)/Ag (100 nm).

(3) HODs: ITO (110 nm)/HTL (or HIL/HTL)/QDs (20 nm)/CBP (40 nm)/MoO_3 (8 nm)/Al (100 nm); HTL (35 nm): TFB, PTAA:TFB, or PTAA:TFB:F4-TCNQ; HIL (40 nm)/HTL (40 nm): PEDOT:PSS/TFB (CBP: 4,4'-bis(9-carbazolyl)-biphenyl).

4.2 Device fabrication

4.2.1 Trilayer PIN QLED

The patterned ITO glass substrates, with a sheet resistance of 25 Ω/□, were first cleaned in an ultrasonic bath for 30 min in detergent and deionized water, respectively. After that, the cleaned ITO substrates were treated with an O_2 plasma for 10 min, and then transferred into a nitrogen-filled glove box to fabricate subsequent functional layers. For ternary BHJ HTL fabrication, the mixed solutions of PTAA (M_W: 15,000–25,000, obtained from Aladdin Scientific Corp.), TFB (M_W > 30,000, obtained from American Dye Source, Inc.), and F4-TCNQ (M_W: 276.15; purity: 97%, obtained from Aladdin Scientific Corp.), with the PTAA:TFB:F4-TCNQ ratio of 28.50:71.25:0.25 were prepared by mixing the 8 mg/mL PTAA solution (in chlorobenzene), 8 mg/mL TFB solution (in chlorobenzene) and/or 2 mg/mL F4-TCNQ solution (acetonitrile). For binary BHJ HTL fabrication, the mixed solutions of PTAA and TFB, with the PTAA:TFB ratio of 0.4:1 were prepared by mixing the 8 mg/mL PTAA solution (in chlorobenzene) and 8 mg/mL TFB solution (in chlorobenzene). For TFB HTL fabrication, the 8 mg/mL TFB solution (in chlorobenzene) was prepared. After solution preparation, they were spin-coated at 3000 rpm for 45 s, followed by annealing at 120 °C for 15 min to form different HTL. After HTL fabrication, 15 mg/mL red QDs (CdZnSe/ZnS/OT, obtained from Mesolight Inc.) solution (in octane) was spin-coated at 1500 rpm for 40 s and baked at 100 °C for 5 min to form the QDs-EML. After EML fabrication, the ZnMgO ETL was prepared by spin-coating the 20 mg/mL $Zn_{0.85}Mg_{0.15}O$ nanoparticle solution (dissolved in ethanol, obtained from Guangdong Poly Optoelectronics Co., Ltd.) at 2000 rpm for 45 s and then annealed at 100 °C for 10 min. Finally, Al cathode (100 nm) was deposited in a high vacuum evaporation chamber with a base pressure of 5×10^{-4} Pa.

4.2.2 Control QLED

The fabrication process of control QLED is identical to the trilayer PIN QLED, except for the PEDOT:PSS HIL. The PEDOT:PSS HIL was fabricated by spin-coating a PEDOT:PSS (Clevios AI 4083) solution at 3000 rpm for 45 s, followed by annealing at 130 °C for 30 min (in air).

4.2.3 HODs

Except for CBP and MoO_3, the fabrication process of other functional layers is the same as that of trilayer PIN QLED or control QLED. The CBP (40 nm) and MoO_3 (8 nm) were deposited sequentially in a high vacuum evaporation chamber with a base pressure of 5×10^{-4} Pa.

4.3 Device characterization

The cross-sectional TEM and elemental mapping results of trilayer PIN QLED were detected by a high-resolution (HR)-TEM (FEI Talos F200X G2), and the samples were sliced via a focused ion beam system (FEI Talos F200X G2). The work functions of the samples were characterized by using a Kelvin probe (KP Technology, APS04-N2-RH). The AFM images of all the organic films were obtained by using an MFP-3D-SA AFM system (Asylum Research). The 2D GIWAXS patterns were carried out by a Xeuss 2.0 instrument (Xenocs, French). The ultraviolet photoelectron spectroscopy (UPS) results of the samples were obtained by using a Thermo Fisher Scientific NEXSA system. The time resolved photoluminescence (TRPL) spectra were detected by the Edinburgh FS5 spectrofluorometer. The thicknesses of all solution-processed films were examined via a Bruker DektakXT stylus profiler. The operational lifetimes of the devices were measured by using a

lifetime measurement system of multi-channel light emitting devices (XP-LTS-8, China). The *J*–*V*–*L*, EQE–*J*, CE–*J*, and PE–*J* curves were measured by using a dual-channel Keithley 2614B programmable source meter with a calibrated PIN-25D silicon photodiode.

Electronic Supplementary Material: Supplementary material ((1) detailed EDS analysis of the device structure; (2) characterization results of the HTLs: photographs, AFM images, energy levels, transmittance spectra, and GIWAXS patterns; (3) *L*–*V*, CE–*J*, and PE–*J* characteristics of trilayer PIN QLEDs and control QLEDs; (4) detailed optimization process of the PTAA:TFB:F4-TCNQ ratio) is available in the online version of this article at https://doi.org/10.26599/NR.2025.94907155.

Data availability

All data needed to support the conclusions in the paper are presented in the manuscript and the Electronic Supplementary Material. Additional data related to this paper may be requested from the corresponding author upon request.

Acknowledgements

This work was supported by the National Natural Science Foundation of China (No. 62304059), the Guangxi Natural Science Foundation (No. 2024GXNSFBA010355), and the Scientific and Technological Bases and Talents of Guangxi (No. Guike AD23026304).

Declaration of competing interest

All the contributing authors report no conflict of interests in this work.

Author contribution statement

H. Z.: Project administration, writing manuscript, funding acquisition. Z. W.: Data curation, experimental design, validation. D. W. Y.: Data curation, validation. B. S. Z.: Project administration, writing manuscript. S. M. C.: Experimental design, writing manuscript. All the authors have approved the final manuscript.

Use of AI statement

None.

References

[1] Alivisatos, A. P. Semiconductor clusters, nanocrystals, and quantum dots. *Science* **1996**, *271*, 933–937.

[2] Kim, T.; Kim, K. H.; Kim, S.; Choi, S. M.; Jang, H.; Seo, H. K.; Lee, H.; Chung, D. Y.; Jang, E. Efficient and stable blue quantum dot light-emitting diode. *Nature* **2020**, *586*, 385–389.

[3] Mashford, B. S.; Stevenson, M.; Popovic, Z.; Hamilton, C.; Zhou, Z. Q.; Breen, C.; Steckel, J.; Bulovic, V.; Bawendi, M.; Coe-Sullivan, S. et al. High-efficiency quantum-dot light-emitting devices with enhanced charge injection. *Nat. Photonics* **2013**, *7*, 407–412.

[4] Qian, L.; Zheng, Y.; Xue, J. E.; Holloway, P. H. Stable and efficient quantum-dot light-emitting diodes based on solution-processed multilayer structures. *Nat. Photonics* **2011**, *5*, 543–548.

[5] Yang, Y. X.; Zheng, Y.; Cao, W. R.; Titov, A.; Hyvonen, J.; Manders, J. R.; Xue, J. E.; Holloway, P. H.; Qian, L. High-efficiency light-emitting devices based on quantum dots with tailored nanostructures. *Nat. Photonics* **2015**, *9*, 259–266.

[6] Shirasaki, Y.; Supran, G. J.; Bawendi, M. G.; Bulović, V. Emergence of colloidal quantum-dot light-emitting technologies. *Nat. Photonics* **2013**, *7*, 13–23.

[7] Choi, M. K.; Yang, J.; Kang, K.; Kim, D. C.; Choi, C.; Park, C.; Kim, S. J.; Chae, S. I.; Kim, T. H.; Kim, J. H. et al. Wearable red-green-blue quantum dot light-emitting diode array using high-resolution intaglio transfer printing. *Nat. Commun.* **2015**, *6*, 7149.

[8] Kim, D. C.; Yun, H.; Kim, J.; Seung, H.; Yu, W. S.; Koo, J. H.; Yang, J.; Kim, J. H.; Hyeon, T.; Kim, D. H. Three-dimensional foldable quantum dot light-emitting diodes. *Nat. Electron.* **2021**, *4*, 671–680.

[9] Shen, H. B.; Gao, Q.; Zhang, Y. B.; Lin, Y.; Lin, Q. L.; Li, Z. H.; Chen, L.; Zeng, Z. P.; Li, X. G.; Jia, Y. et al. Visible quantum dot light-emitting diodes with simultaneous high brightness and efficiency. *Nat. Photonics* **2019**, *13*, 192–197.

[10] Gao, Y.; Li, B.; Liu, X. N.; Shen, H. B.; Song, Y.; Song, J. J.; Yan, Z. J.; Yan, X. H.; Chong, Y. H.; Yao, R. Y. et al. Minimizing heat generation in quantum dot light-emitting diodes by increasing quasi-fermi-level splitting. *Nat. Nanotechnol.* **2023**, *18*, 1168–1174.

[11] Deng, Y. Z.; Peng, F.; Lu, Y.; Zhu, X. T.; Jin, W. X.; Qiu, J.; Dong, J. W.; Hao, Y. L.; Di, D. W.; Gao, Y. et al. Solution-processed green and blue quantum-dot light-emitting diodes with eliminated charge leakage. *Nat. Photonics* **2022**, *16*, 505–511.

[12] Chen, X. T.; Lin, X. F.; Zhou, L. K.; Sun, X. J.; Li, R.; Chen, M. Y.; Yang, Y. X.; Hou, W. J.; Wu, L. J.; Cao, W. R. et al. Blue light-emitting diodes based on colloidal quantum dots with reduced surface-bulk coupling. *Nat. Commun.* **2023**, *14*, 284.

[13] Zhang, W. J.; Li, B.; Chang, C.; Chen, F.; Zhang, Q.; Lin, Q. L.; Wang, L.; Yan, J. H.; Wang, F. F.; Chong, Y. H. et al. Stable and efficient pure blue quantum-dot LEDs enabled by inserting an anti-oxidation layer. *Nat. Commun.* **2024**, *15*, 783.

[14] Lee, T.; Kim, B. J.; Lee, H.; Hahm, D.; Bae, W. K.; Lim, J.; Kwak, J. Bright and stable quantum dot light-emitting diodes. *Adv. Mater.* **2022**, *34*, 2106276.

[15] Dai, X. L.; Deng, Y. Z.; Peng, X. G.; Jin, Y. Z. Quantum-dot light-emitting diodes for large-area displays: Towards the dawn of commercialization. *Adv. Mater.* **2017**, *29*, 1607022.

[16] Chen, Z. N.; Li, H. T.; Yuan, C. X.; Gao, P. L.; Su, Q.; Chen, S. M. Color revolution: Prospects and challenges of quantum-dot light-emitting diode display technologies. *Small Methods* **2024**, *8*, 2300359.

[17] Hong, G.; Gan, X. M.; Leonhardt, C.; Zhang, Z.; Seibert, J.; Busch, J. M.; Bräse, S. A brief history of OLEDs-emitter development and industry milestones. *Adv. Mater.* **2021**, *33*, 2005630.

[18] Baldo, M. A.; Thompson, M. E.; Forrest, S. R. High-efficiency fluorescent organic light-emitting devices using a phosphorescent sensitizer. *Nature* **2000**, *403*, 750–753.

[19] Kim, J. U.; Park, I. S.; Chan, C. Y.; Tanaka, M.; Tsuchiya, Y.; Nakanotani, H.; Adachi, C. Nanosecond-time-scale delayed fluorescence molecule for deep-blue OLEDs with small efficiency rolloff. *Nat. Commun.* **2020**, *11*, 1765.

[20] Dai, X. L.; Zhang, Z. X.; Jin, Y. Z.; Niu, Y.; Cao, H. J.; Liang, X. Y.; Chen, L. W.; Wang, J. P.; Peng, X. G. Solution-processed, high-performance light-emitting diodes based on quantum dots. *Nature* **2014**, *515*, 96–99.

[21] Yang, C. Y.; Ma, R.; Wang, Z.; Wang, Y. Y.; Yu, C. Y.; Liu, Y. G.; Wan, Y. F.; Li, J. F.; Tong, J. F.; Zhang, P. et al. Efficient quantum dot light-emitting diode enabled by a thick inorganic CdS interfacial modification layer. *ACS Appl. Mater. Interfaces* **2023**, *15*, 54185–54191.

[22] Sun, Y. Z.; Jiang, Y. B.; Peng, H. R.; Wei, J. L.; Zhang, S. D.; Chen, S. M. Efficient quantum dot light-emitting diodes with a $Zn_{0.85}Mg_{0.15}O$ interfacial modification layer. *Nanoscale* **2017**, *9*, 8962–8969.

[23] Cameron, J.; Skabara, P. J. The damaging effects of the acidity in PEDOT:PSS on semiconductor device performance and solutions based on non-acidic alternatives. *Mater. Horiz.* **2020**, *7*, 1759–1772.

[24] Phan, T. N. L.; Kim, J.; Kim, G. U.; Lee, S.; Kim, B. J. Aniline-based hole transporting materials for high-performance organic solar cells with enhanced ambient stability. *J. Mater. Chem. A* **2021**, *9*, 15787–15797.

[25] Kawano, K.; Pacios, R.; Poplavskyy, D.; Nelson, J.; Bradley, D. D. C.; Durrant, J. R. Degradation of organic solar cells due to air exposure. *Solar Energy Mater. Solar Cells* **2006**, *90*, 3520–3530.

[26] Yang, X. Y.; Mutlugun, E.; Zhao, Y. B.; Gao, Y.; Leck, K. S.; Ma, Y. Y.; Ke, L.; Tan, S. T.; Demir, H. V.; Sun, X. W. Solution processed tungsten oxide interfacial layer for efficient hole-injection in quantum dot light-emitting diodes. *Small* **2014**, *10*, 247–252.

[27] Zhang, H.; Sun, X. W.; Chen, S. M. Over 100 cd A^{-1} efficient quantum dot light-emitting diodes with inverted tandem structure. *Adv. Funct. Mater.* **2017**, *27*, 1700610.

[28] Wang, F. Z.; Wang, Z. Y.; Zhu, X. D.; Bai, Y. M.; Yang, Y., Hu, S. Q.; Liu, Y. Q.; You, B. G.; Wang, J.; Li, Y. et al. Highly efficient and super stable full-color quantum dots light-emitting diodes with solution-processed all-inorganic charge transport layers. *Small* **2021**, *17*, 2007363.

[29] Pu, C. D.; Dai, X. L.; Shu, Y. F.; Zhu, M. Y.; Deng, Y. Z.; Jin, Y. Z.; Peng, X. G. Electrochemically-stable ligands bridge the photoluminescence-electroluminescence gap of quantum dots. *Nat. Commun.* **2020**, *11*, 937.

[30] Chen, D. S.; Chen, D.; Dai, X. L.; Zhang, Z. X.; Lin, J.; Deng, Y. Z.; Hao, Y. L.; Zhang, C.; Zhu, H. M.; Gao, F. et al. Shelf-stable quantum-dot light-emitting diodes with high operational performance. *Adv. Mater.* **2020**, *32*, 2006178.

[31] Cao, W. R.; Xiang, C. Y.; Yang, Y. X.; Chen, Q.; Chen, L. W.; Yan, X. L.; Qian, L. Highly stable QLEDs with improved hole injection via quantum dot structure tailoring. *Nat. Commun.* **2018**, *9*, 2608.

[32] Chen, S.; Cao, W. R.; Liu, T. L.; Tsang, S. W.; Yang, Y. X.; Yan, X. L.; Qian, L. On the degradation mechanisms of quantum-dot light-emitting diodes. *Nat. Commun.* **2019**, *10*, 765.

[33] Greiner, M. T.; Helander, M. G.; Tang, W. M.; Wang, Z. B.; Qiu, J.; Lu, Z. H. Universal energy-level alignment of molecules on metal oxides. *Nat. Mater.* **2012**, *11*, 76–81.

[34] Zhang, H.; Wang, S. T.; Sun, X. W.; Chen, S. M. Solution-processed vanadium oxide as an efficient hole injection layer for quantum-dot light-emitting diodes. *J. Mater. Chem. C* **2017**, *5*, 817–823.

[35] Nie, L. T.; Fan, J. P.; Li, Y. B.; Xiang, C. Y.; Zhang, T. Direct optical patterning of MoO_3 nanoparticles and their application as a hole injection layer for solution-processed quantum dot light-emitting diodes. *ACS Appl. Nano Mater.* **2024**, *7*, 9499–9506.

[36] Yang, X. Y.; Ma, Y. Y.; Mutlugun, E.; Zhao, Y. B.; Leck, K. S.; Tan, S. T.; Demir, H. V.; Zhang, Q. Y.; Du, H. J.; Sun, X. W. Stable, efficient, and all-solution-processed quantum dot light-emitting diodes with double-sided metal oxide nanoparticle charge transport layers. *ACS Appl. Mater. Interfaces* **2014**, *6*, 495–499.

[37] Wan, H. Y.; Jung, E. D.; Zhu, T.; Park, S. M.; Pina, J. M.; Xia, P.; Bertens, K.; Wang, Y. K.; Atan, O.; Chen, H. J. et al. Nickel oxide hole injection layers for balanced charge injection in quantum dot light-emitting diodes. *Small* **2024**, *20*, 2402371.

[38] Lin, J.; Dai, X. L.; Liang, X. Y.; Chen, D. S.; Zheng, X. R.; Li, Y. F.; Deng, Y. Z.; Du, H.; Ye, Y. X.; Chen, D. et al. High-performance quantum-dot light-emitting diodes using NiO_x hole-injection layers with a high and stable work function. *Adv. Funct. Mater.* **2020**, *30*, 1907265.

[39] Caruge, J. M.; Halpert, J. E.; Wood, V.; Bulović, V.; Bawendi, M. G. Colloidal quantum-dot light-emitting diodes with metal-oxide charge transport layers. *Nat. Photonics* **2008**, *2*, 247–250.

[40] Lei, S. Y.; Xiao, Y. Y.; Yu, K. L.; Xiao, B.; Wan, M.; Zou, L. Y.; You, Q. L.; Yang, R. Q. Revisiting hole injection in quantum dot light-emitting diodes. *Adv. Funct. Mater.* **2023**, *33*, 2305732.

[41] Su, Q.; Zhang, H.; Chen, S. M. Identification of excess charge carriers in InP-based quantum-dot light-emitting diodes. *Appl. Phys. Lett.* **2020**, *117*, 053502.

[42] Kim, J.; Hahm, D.; Bae, W. K.; Lee, H.; Kwak, J. Transient dynamics of charges and excitons in quantum dot light-emitting diodes. *Small* **2022**, *18*, 2202290.

[43] Liao, Z. B.; Mallem, K.; Prodanov, M. F.; Kang, C. B.; Gao, Y. Y.; Song, J. X.; Vashchenko, V. V.; Srivastava, A. K. Ultralow roll-off quantum dot light-emitting diodes using engineered carrier injection layer. *Adv. Mater.* **2023**, *35*, 2303950.

[44] Bao, H.; Chen, C. L.; Cao, Y. Q.; Chang, S.; Wang, S. P.; Zhong, H. Z. Quantitative determination of charge accumulation and recombination in operational quantum dots light emitting diodes via time-resolved electroluminescence spectroscopy. *J. Phys. Chem. Lett.* **2023**, *14*, 1777–1783.